Stimulated Raman scattering from free holes in p-type indium antimonide

R. Ebert,* H. Pascher, and H. G. Häfele
Physikalisches Institut, Universität Würzburg, D-8700 Würzburg, Federal Republic of Germany
(Received 9 September 1980)

Stimulated Raman scattering from photoexcited holes at magnetic fields up to 68 kG in p-InSb is described. Experiments varying excitation wavelength, magnetic field, polarization, and sample orientation are discussed. A comparison of the experimental results with the latest valence-band calculations allows the identification of the energy levels involved in the scattering process. For sample orientation $\vec{H}\|\langle 100\rangle$, the initial state is the valence-band Landau level ALH $1_0 1^+ 31$ and the final state is BHH $3_1 3^- 31$. ALH, BLH are the "light hole" ladders (approximate spin $M = +3/2$ and $M = -3/2$, respectively). AHH, BHH are the "heavy hole" ladders (approximate spin $M = -1/2$ and $M = +1/2$, respectively). For the orientation $\vec{H}\|\langle 111\rangle$ initial state and final state are BLH $0_0 0^+$ and AHH $3_2 0^+$, respectively. The holes involved in this Raman scattering process always have a nonzero momentum along the direction of the magnetic field ($k_H \neq 0$). The largest Raman shift we measured was about 2.7 cm^{-1}.

I. INTRODUCTION

Spin-flip Raman scattering from holes in the valence band of a semiconductor was first considered theoretically by Yafet in 1966.[1] The scattering process he described takes place in the degenerated valence-band energy levels which are split apart by the application of a magnetic field. Hollis and Scott[2] reported the first time on spin-flip scattering in the valence band. They observed spontaneous spin-flip Raman scattering from free holes in p-ZnTe. We reported the first time on stimulated Raman scattering from photoexcited holes and electrons in p-InSb.[3] The Raman scattering from photoexcited electrons, which turned out to be a spin-flip scattering, showed in almost every detail the same behavior as the spin-flip Raman scattering from conduction electrons in very pure n-type InSb. Thus in this paper we are concerned with the more interesting scattering process from photoexcited holes in the complex valence-band energy levels. To give a complete interpretation of the experimental results, especially of the magnetic field dependence of the Raman shift, we did further experiments which, in connection with the latest valence-band calculations of InSb by Trebin and Rössler,[4] led us to an understanding of the behavior of this scattering process.

In the very latest publication,[5] Scott gives a totally different explanation of our first published data[3] than that which we propose. He reanalyzed our data of Ref. 3 in terms of free-to-bound exciton transitions. Stimulated by that paper we have done further experiments which confirm our interpretation.

II. EXPERIMENTAL DETAILS

The samples used were cut from single crystals of p-type InSb with carrier concentrations of $p \equiv (N_A - N_D) = 1.6 \times 10^{13}$ cm^{-3}, $p = 1.0 \times 10^{14}$ cm^{-3}. Sample dimensions were $3 \times 3 \times 8$ mm^3. We investigated the scattering process for three different sample orientations in the magnetic field: $\vec{H}\|\langle 100\rangle$, $\vec{H}\|\langle 110\rangle$, and $\vec{H}\|\langle 111\rangle$. The samples were immersed in superfluid helium pumped to a temperature of 1.6 K. As pump laser we used a Q-switched low-pressure CO laser. A grating selected one of the emitted laser lines. Typical output powers for the laser lines used were about 100 W. The pulse widths were ≈100 nsec and the repetition rate was about 200 Hz. The CO-laser beam was focussed onto the sample with a CaF_2 lens ($f = 30$ cm) with the sample mounted in the Voigt configuration in the center of a 68-kG split-coil superconducting magnet. The transmitted and scattered radiation was detected with an InSb detector in conjunction with an $f/6$ grating spectrometer and the signal was then fed into a boxcar integrator and recorded. The standard deviation of our frequency measurements by the spectrometer was ±0.05 cm^{-1}.

III. THEORETICAL BACKGROUND

Yafet[1] calculated the cross sections for Raman scattering by electrons and holes in a semiconductor subjected to a magnetic field. He predicted that the cross section will diverge as the laser energy approaches the band-gap energy. If you want to discuss Raman scattering processes, especially Raman scattering by holes, it is necessary to have an exact model of the Landau states because of the complex valence-band structure in InSb.

A very extensive and detailed calculation of the Landau states of InSb was done by Trebin and Rössler.[4] The calculation concept is based on an effective Hamiltonian acting in the eightfold space of the valence band and the lowest conduction band

 © 1981 The American Physical Society

TABLE I. Dipole selection rules between Landau levels for inter- and intraband transitions (taken from Ref. 4).

	Relative matrix element		Selection rules											
			$e_\pm$						e_3					
Type	intra	inter	$\Delta\pi$	ΔN	ΔK	ΔQ [001]	ΔQ [110]	ΔP [001]	$\Delta\pi$	ΔN	ΔK	ΔQ [001]	ΔQ [110]	ΔP [001]
M_0	$\gamma_1,\gamma_2,\gamma_3$	p_s	yes	±1	±1	±1	0	1	yes	0	0	2	1	0
M_1	$\gamma_2\zeta,\gamma_3\zeta$	$p_s\zeta$		±1	±1			1		0	0			0
M_2	$\gamma_2-\gamma_3$		yes		±1	±1	0	1	yes		0	2	1	0
M_3	$(\gamma_2-\gamma_3)\zeta$				±1			1			0			0
M_4	c, c_4, c_5'	b, c_2T			(±1)	±1	0	1			(0)	2	1	0
M_5	$c\zeta, c_4\zeta, c_5\zeta$	$b\zeta$	"yes"		(±1)			1	"yes"		(0)			0

of a zinc-blende-type material. The Hamiltonian is constructed by invariant expansion. The method of invariants, which has been successfully applied to germanium by Hensel and Suzuki,[6] is extended to the cross space between valence band and conduction band on the basis of the angular momentum calculus. The schemes for the classification of the energy levels are established according to the transformation properties of the eigenstates since the Hamiltonian is constructed on group-theoretical considerations. In Table I (taken from Ref. 4) selection rules are given for inter- and intraband transitions for circulary polarized ($e_\pm$) and longitudinal (e_3) electric fields. Apart from the M_0-type transitions, which are always present and presumed to be the strongest, several less restrictive selection rules are given: The M_1-type transitions are possible only through the longitudinal momentum k_H and hence they are referred to as noncentral or k_H transitions, M_2-type transitions are harmonic or warping-induced transitions, M_3-type transitions are k_H-harmonic transitions, M_4-type transitions are inversion-asymmetry-induced transitions, and M_5-type transitions are k_H-inversion-asymmetry-induced transitions. (A complete explanation of these types of transitions and of the quantum numbers used is given by Trebin *et al.*[4])

By spin-flip transitions in the valence band we denote those processes which involve one photon polarized parallel to the magnetic field H and one-polarized transverse to H. Owing to this definition of a spin-flip scattering process in the valence band given by Yafet[1] you can, with the assistance of Table I, set up the selection rules for spin-flip scattering processes in the valence band as well as in the conduction band.

Table II shows the selection rules for spin-flip Raman (SFR) scattering processes in the conduction and valence band. For the transitions from the initial to the intermediate states and from there to the final state we assumed M_0-type tran-

TABLE II. Selection rules for the spin-flip Raman scattering in the conduction band and valence band.

			$\vec{e}_P\perp\vec{H}$; $\vec{e}_S\parallel\vec{H}$ or $\vec{e}_P\parallel\vec{H}$; $\vec{e}_S\perp\vec{H}$		
$\Delta\pi$	ΔN	ΔK	$\Delta Q\,\langle100\rangle$	$\Delta Q\,\langle110\rangle$	$\Delta P\,\langle100\rangle$
no	±1	±1	±1	±1	±1

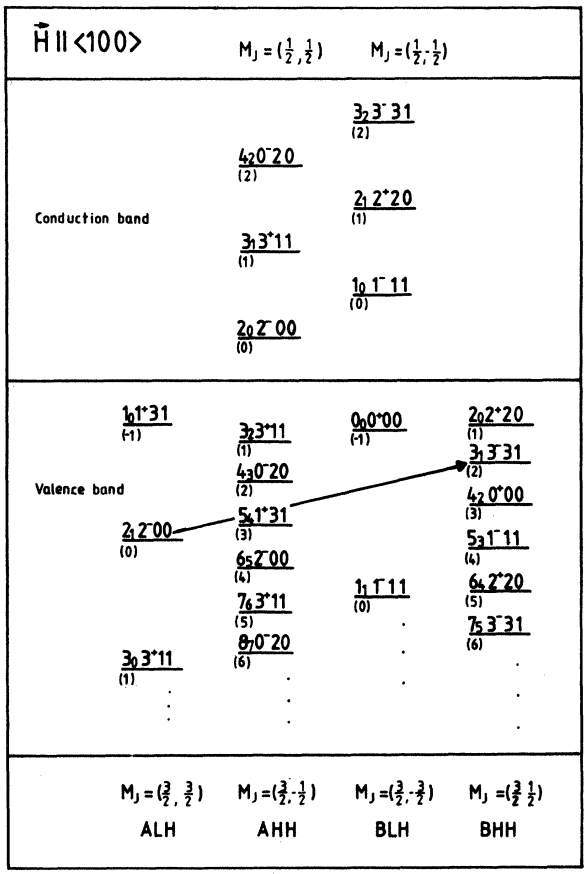

FIG. 1. Classification of the energy levels of the conduction band and valence band for $\vec{H}\parallel\langle100\rangle$. The arrow marks a possible spin-flip transition in the valence band according to Table II.

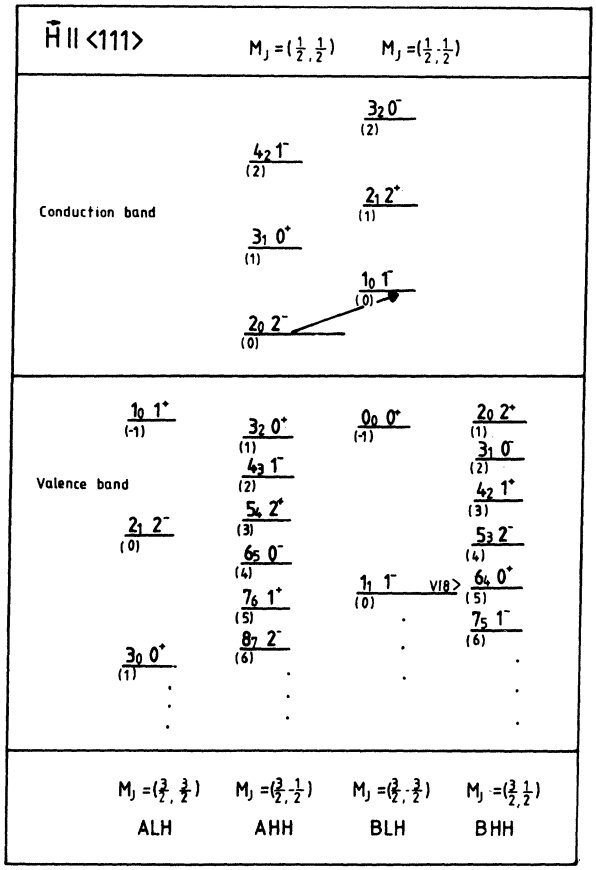

FIG. 2. Classification of the energy levels of the conduction band and valence band for $\vec{H} \parallel \langle 111 \rangle$. The arrow marks a possible spin-flip transition in the conduction band according to Table II.

sitions.

In Figs. 1 and 2, the energy levels for the magnetic field orientations $\vec{H} \parallel \langle 100 \rangle$ and $\vec{H} \parallel \langle 111 \rangle$ are sketched and possible SFR transitions in the conduction and in the valence band are marked. Since it is convenient we describe the hole scattering in the valence band by the movement of the corresponding electron (electron picture). The notation of the energy level is taken from Trebin *et al.*[4] The quantum numbers in round brackets are according to the work of Pidgeon and Brown,[7] which allow a comparison with the notation of Trebin *et al.*

As you will see later, our experimental results could *not* be interpreted by such Raman hole scattering processes in the valence band shown in Fig. 1. So we have taken into consideration Raman scattering by holes with nonzero longitudinal momentum k_H. Figure 3 shows the k_H dependence of

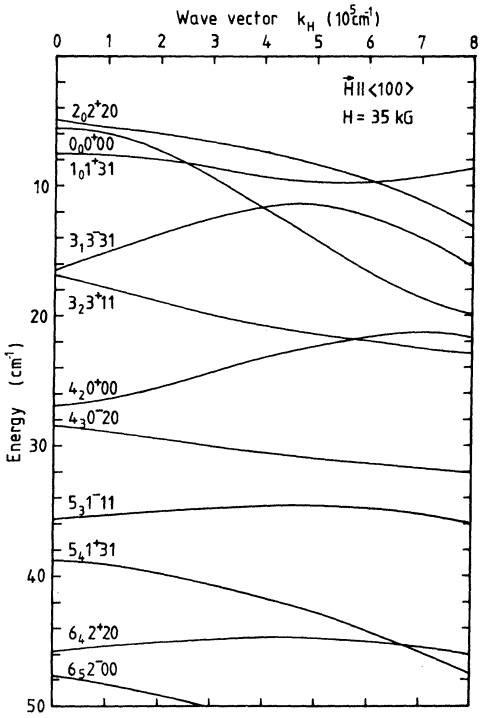

FIG. 3. k_H dependence of the first eleven valence-band levels for $\vec{H} \parallel \langle 100 \rangle$ at a magnetic field of 35 kG.

the first eleven valence-band energy levels in the presence of a magnetic field, which is 35 kG and has the orientation $\vec{H} \parallel \langle 100 \rangle$.

These valence-band calculations have been done by a calculation program Trebin had placed at our disposal. We should like to remark that the band

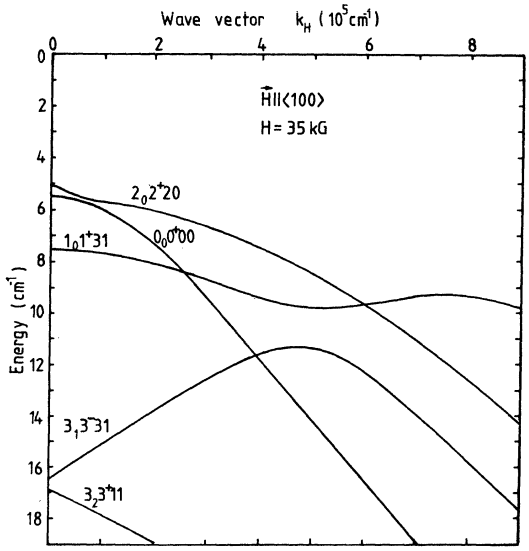

FIG. 4. k_H dependence of the first five valence-band levels for $\vec{H} \parallel \langle 100 \rangle$ at a magnetic field of 35 kG.

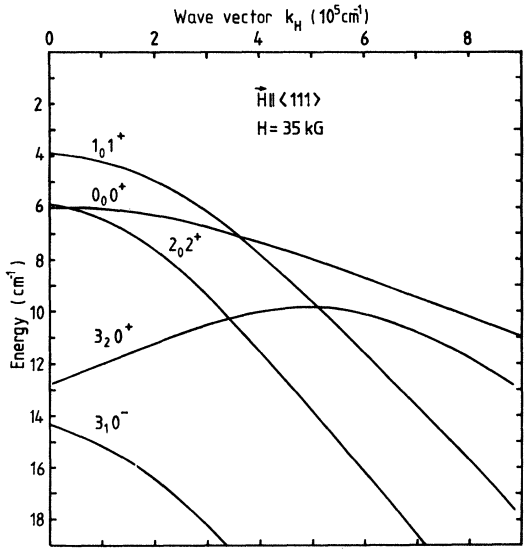

FIG. 5. k_H dependence of the first five valence-band levels for $\vec{H}\|\langle 111\rangle$ at a magnetic field of 35 kG.

parameters used ($\gamma_1 = 40.0$, $\gamma_2 = 18.0$, $\gamma_3 = 19.2$, $\kappa = 17.1$, and $q = 0.4$) were determined from cyclotron resonance measurements by Ranvaud,[8] and not just fitted to our data.

Because of the complex k_H dependence of the valence-band energy levels in the magnetic field it is necessary to restrict our discussion to those levels which could, with respect to the given experimental situation, be involved in Raman scattering processes from holes.

Figures 4 and 5 show the first five valence-band energy levels at a magnetic field of 35 kG, with k_H values up to 8×10^5 cm^{-1}, and for the magnetic field orientations $\vec{H}\|\langle 100\rangle$ and $\vec{H}\|\langle 111\rangle$, respectively. (No calculation was done for the magnetic field orientation $\vec{H}\|\langle 110\rangle$ and $k_H \neq 0$ because the Hamiltonian of the $\langle 110\rangle$ direction has only the

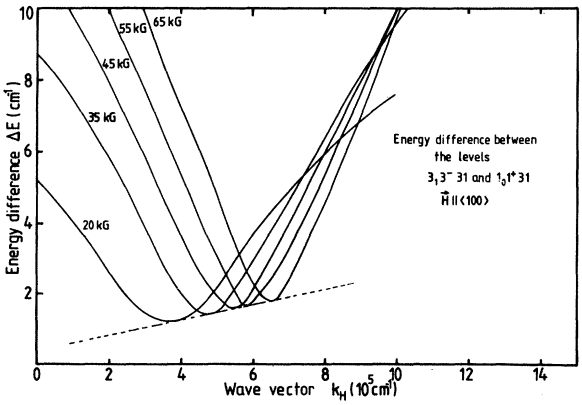

FIG. 6. k_H dependence of the energy difference between the valence-band levels $3_1 3^- 31$ and $1_0 1^+ 31$ for five different magnetic fields ($\vec{H}\|\langle 100\rangle$).

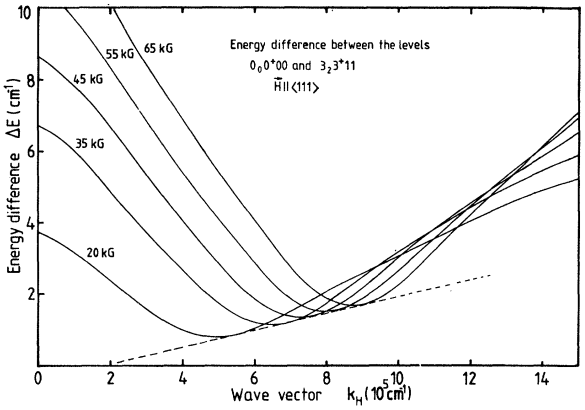

FIG. 7. k_H dependence of the energy difference between the valence-band levels $0_0 0^+00$ and $3_2 3^+11$ for five different magnetic fields ($\vec{H}\|\langle 111\rangle$).

trivial symmetry so that the full Hamiltonian matrix has to be diagonalized.) Energy levels with different quantum numbers K (for $\vec{H}\|\langle 111\rangle$) or different quantum numbers P (for $\vec{H}\|\langle 100\rangle$) cross, while those with same K or P repel as they approach one another in the diagram (Figs. 4 and 5) in which the levels are plotted as function of k_H. The valence-band energy levels $1_0 1^+31$ and $3_1 3^-31$ for $\vec{H}\|\langle 100\rangle$, as well as $0_0 0^+$ and $3_2 0^+$ for $\vec{H}\|\langle 111\rangle$ show this anticrossing behavior very clearly (see Figs. 4 and 5).

Another interesting fact is that the energy distance between these levels in the anticrossing region increases very slowly with increasing the magnetic field. Figures 6 and 7 show the energy differences of the two energy levels concerned for

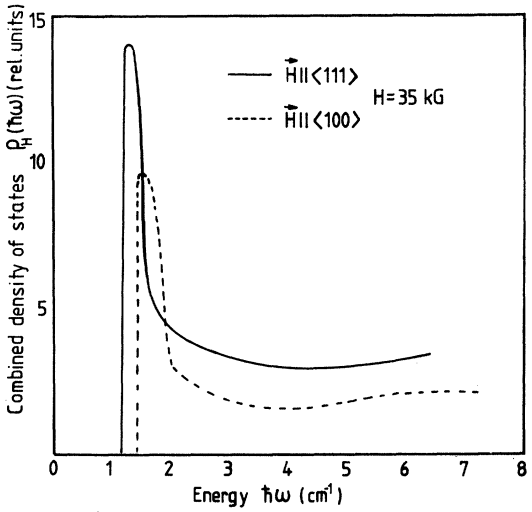

FIG. 8. Combined density of states of the levels $3_1 3^- 31$ and $1_0 1^+ 31$ for $\vec{H}\|\langle 100\rangle$, and of the levels $0_0 0^+00$ and $3_2 3^+11$ for $\vec{H}\|\langle 111\rangle$.

five different magnetic field values for $\vec{H} \parallel \langle 100 \rangle$ and $\vec{H} \parallel \langle 111 \rangle$, respectively. It is obvious from Figs. 6 and 7 that the energy differences of the energy levels near the anticrossing points remain almost constant respecting the large magnetic field region of 35 to 65 kG. For an increasing magnetic field the points where the levels approach one another are shifted to larger k_H values. Furthermore, in the k_H region where the levels approach one another, the curves of the two energy levels become parallel, which points to a large combined density of states.

According to Eq. (1), which gives the combined density of states without consideration of any quenching effects, we calculated the combined density of states of the energy levels for $\vec{H} \parallel \langle 100 \rangle$ and $\vec{H} \parallel \langle 111 \rangle$ as follows:

$$\rho_H(\hbar\omega) = \frac{eH}{(2\pi)^2\hbar} \left| \frac{1}{\frac{\partial E_1}{\partial k_H} - \frac{\partial E_2}{\partial k_H}} \right|_{E_1(k_H) - E_2(k_H) = \hbar\omega} . \quad (1)$$

$E_1(k_H)$ is the energy of the levels $1_0 1^+ 31$ for $\vec{H} \parallel \langle 100 \rangle$ and $0_0 0^+$ for $\vec{H} \parallel \langle 111 \rangle$ in dependence of k_H. $E_2(k_H)$ is the energy of the levels $3_1 3^- 31$ for $\vec{H} \parallel \langle 100 \rangle$ and $3_2 0^+$ for $\vec{H} \parallel \langle 111 \rangle$ in dependence of k_H.

The result of the calculation for $H = 35$ kG is given in Fig. 8. The combined density of states shows peaks centered at 1.3 cm^{-1} for $\vec{H} \parallel \langle 111 \rangle$ and at 1.5 cm^{-1} for $\vec{H} \parallel \langle 100 \rangle$. The next section will show that all these special behaviors of the valence-band energy levels with which we are concerned play an important part in the discussion of our experimental data of the stimulated Raman scattering.

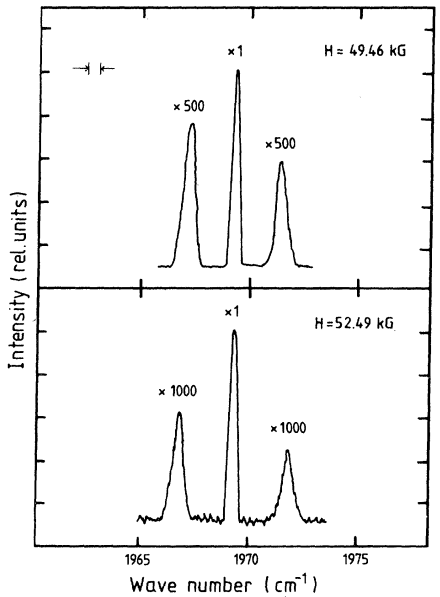

FIG. 9. Spectra of the stimulated Raman scattering from photoexcited holes taken at two different magnetic fields. (InSb, $p = 1 \times 10^{14}$ cm^{-3}, $T = 1.6$ K, pump frequency $\omega_L = 1969.284$ cm^{-1}, polarization: $\vec{E}_L \parallel \vec{H}$).

IV. EXPERIMENTAL RESULTS AND DISCUSSION

First the experimental facts are listed: For magnetic fields >30 kG we observed a Raman scattering process with a very small Raman shift of about 0.2 cm^{-1}/kG. Figure 9 shows two spectra taken at different magnetic fields. We registered Stokes and anti-Stokes lines, the intensity of the Stokes being generally twice that of the anti-Stokes. The nonlinear dependence of the scattered intensity on the pump intensity and its narrow linewidth make it obvious that the scattering process is stimulated. The polarization of the scattered radiation is parallel to the pump laser beam and also parallel to the magnetic field direction. The scattering process is not to be observed at temperatures higher than 2.5 K. The measured frequency shifts were different for different CO-laser pump wavelengths. The frequency shifts did not extrapolate to zero at zero magnetic field.

Figures 10, 11, and 12 show the tuning characteristics of the scattered radiation dependent on the magnetic field for sample orientations $\vec{H} \parallel \langle 100 \rangle$, $\vec{H} \parallel \langle 111 \rangle$, and $\vec{H} \parallel \langle 110 \rangle$. In our first experiments we could observe frequency shifts for seven different CO-laser pump wavelengths (No. 1, 2, 3, 6, 7, 12, and 13), which are the strongest in the frequency region of 1943 to 2008 cm^{-1}. To find out whether the number of the observed transitions is restricted to eight (Scott's theory predicts eight transitions at most[5]), we optimized the CO-laser output for the short wavelengths and repeated the experiments for the $\vec{H} \parallel \langle 100 \rangle$ orientation. We could then observe frequency shifts for fifteen different CO-laser pump wavelengths (see Fig. 10). The spectrum ends at 68 kG because this is the maximum magnetic field we can achieve. We are sure that you can observe even more transitions if higher magnetic fields and shorter CO-laser wavelengths are at your disposal.

There are two experimental data which characterize the anisotropy of the scattered radiation: First, the frequency shifts started at about 1.2 cm^{-1} for $\vec{H} \parallel \langle 111 \rangle$, at about 1.4 cm^{-1} for $\vec{H} \parallel \langle 100 \rangle$, and at 1.7 cm^{-1} for $\vec{H} \parallel \langle 110 \rangle$; second, the observed frequency shifts are shifted to slightly higher fields when you go from $\vec{H} \parallel \langle 110 \rangle$ to $\vec{H} \parallel \langle 100 \rangle$ and further to $\vec{H} \parallel \langle 111 \rangle$.

An interpretation of the experimental data has to explain the facts mentioned above and especially, since we intend to interpret the measurements by stimulated Raman scattering from photoexcited holes in the valence band, this interpretation has

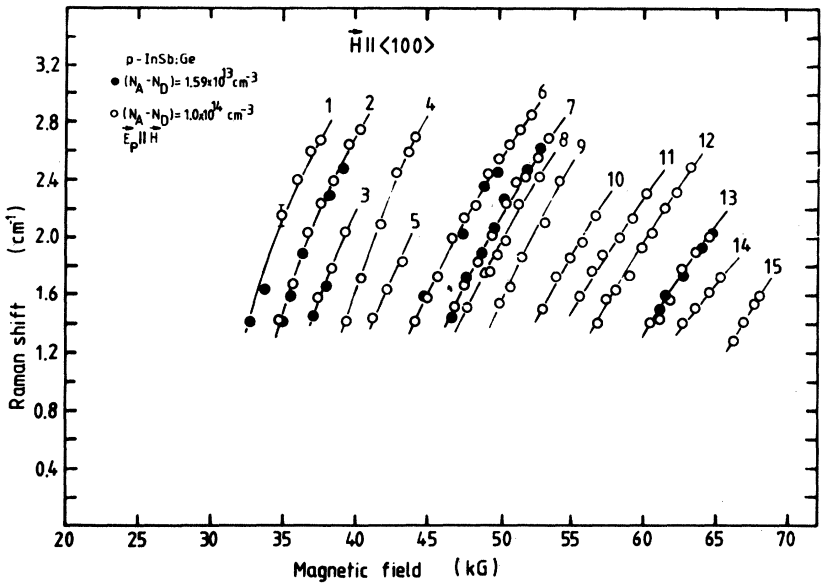

FIG. 10. Magnetic field dependence of the frequency shift of the stimulated Raman scattering from photoexcited holes at various pump frequencies. Magnetic field orientation is $\vec{H} \| \langle 100 \rangle$. ●: InSb, $p=1.6\times10^{13}$ cm^{-3}; ○: InSb, $p=1.0\times10^{14}$ cm^{-3}; curve 1: pump frequency 1943.536 cm^{-1}; curve 2: pump frequency 1947.512 cm^{-1}; curve 3: pump frequency 1951.456 cm^{-1}; curve 4: pump frequency 1957.049 cm^{-1}; curve 5: pump frequency 1961.160 cm^{-1}; curve 6: pump frequency 1965.239 cm^{-1}; curve 7: pump frequency 1969.284 cm^{-1}; curve 8: pump frequency 1973.296 cm^{-1}; curve 9: pump frequency 1977.274 cm^{-1}; curve 10: pump frequency 1982.765 cm^{-1}; curve 11: pump frequency 1986.912 cm^{-1}; curve 12: pump frequency 1991.025 cm^{-1}; curve 13: pump frequency 1995.105 cm^{-1}; curve 14: pump frequency 1999.152 cm^{-1}; curve 15: pump frequency 2008.552 cm^{-1}.

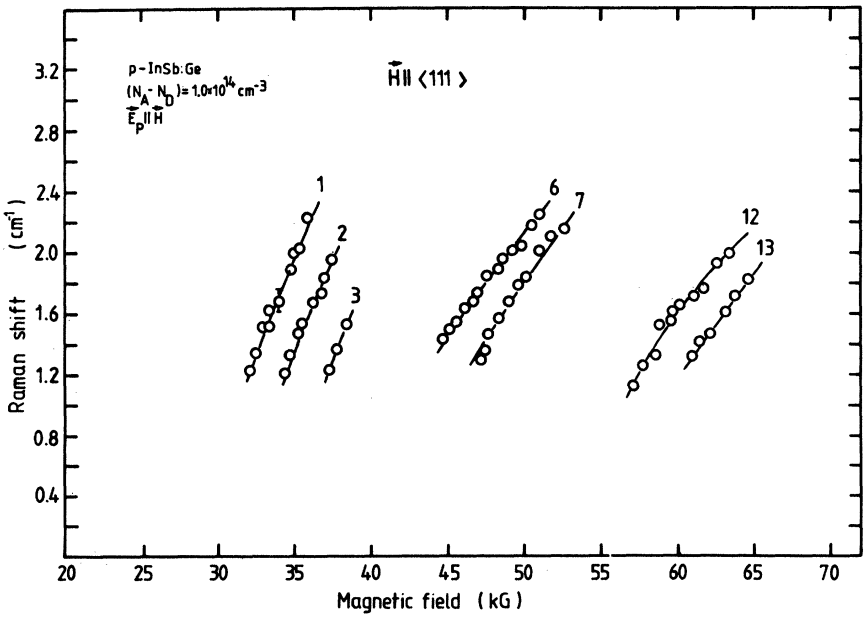

FIG. 11. Magnetic field dependence of the frequency shift of the stimulated Raman scattering from photoexcited holes at various pump frequencies (see also Fig. 10). Magnetic field orientation is $\vec{H} \| \langle 111 \rangle$.

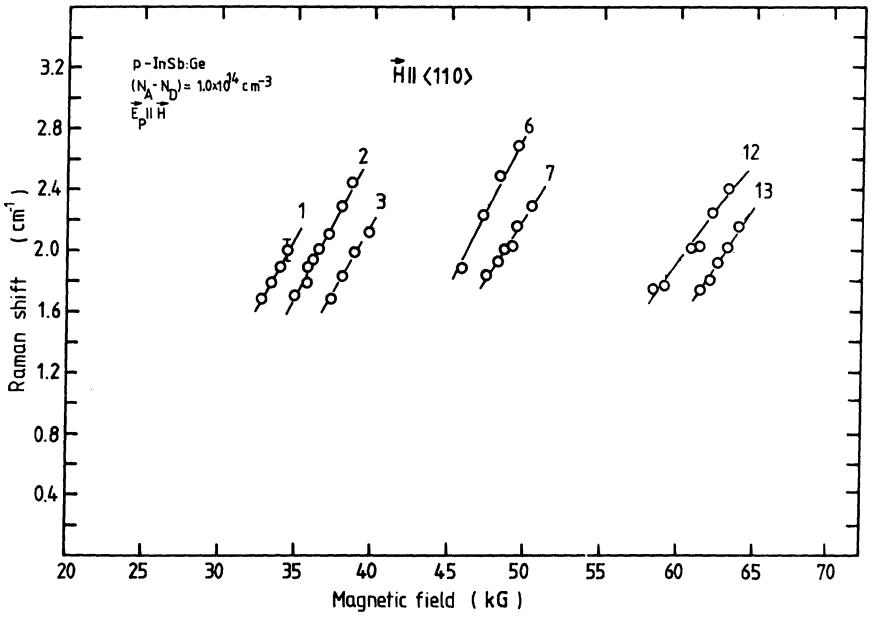

FIG. 12. Magnetic field dependence of the frequency shift of the stimulated Raman scattering from photoexcited holes at various pump frequencies (see also Fig. 10). Magnetic field orientation is $\vec{H} \| \langle 110 \rangle$.

to explain why different pump lines show different tuning characteristics, and why the magnetic field dependence of the scattered radiation starts always with almost the same frequency shift although the magnetic field increases from 30 to 60 kG. All the results can be explained by stimulated Raman scattering from photoexcited holes assuming that this scattering process takes place between the valence-band levels $1_0 1^+ 31$, $3_1 3^- 31$ for $\vec{H} \| \langle 100 \rangle$ and $0_0 0^+$, $3_2 0^+$ for $\vec{H} \| \langle 111 \rangle$ in that k_H region where these levels approach one another (see Figs. 4 and 5). The calculation of the energy difference of the anticrossing levels shows (see Figs. 6 and 7) that the smallest energy difference of these levels is almost constant between 30 and 60 kG. When we assume that the quasi-Fermi level of the photoexcited holes is placed between the respective levels we would expect the scattering process to take place where the combined density of states is largest (see Fig. 8). In this case the energy shift ought to be about 1.3 and 1.5 cm^{-1} for $\vec{H} \| \langle 111 \rangle$ and for $\vec{H} \| \langle 100 \rangle$, respectively. Reference to Figs. 10 and 11 shows that this is in good accord with the transitions observed. Even the small dependence on sample orientations (smaller energy shifts for $\vec{H} \| \langle 111 \rangle$ than for $\vec{H} \| \langle 100 \rangle$ is confirmed by the experimental data. For $\vec{H} \| \langle 110 \rangle$ there is no comparison possible with theoretical calculations since for this orientation no calculation was done as already mentioned in Sec. III.

To give an explanation of the magnetic tuning of energy shifts for each pump laser line you have to take into consideration the magnetic field dependence of the quasi-Fermi level for a given excitation wavelength. The position of the quasi-Fermi level of the photoexcited holes depends on the energy and intensity of the pump wavelength as well as on the magnetic field. It should be noticed that the energy gap of the InSb samples at 1.6 K happens to coincide almost exactly with the energies of the CO-laser lines used. Therefore, the magnetic field dependence of the energy gap affects very strongly the production of the photoexcited holes. From Figs. 6 and 7 there can be seen what happens when the quasi-Fermi level is between the anticrossing levels and the magnetic field is increased. The quasi-Fermi level begins to move towards the top of the valence band (increasing the magnetic field reduces the absorption of the pump laser). The quasi-Fermi level reaches the upper of the anticrossing levels first at that k_H value where they approach one another. The hole population begins to decrease where the energy difference of the anticrossing levels is smallest. Thus, the scattering process is shifted to k_H values in the vicinity of the anticrossing point and leads to larger Raman shifts. So the magnetic tuning behavior of the energy shifts for each of the pump wavelengths depends likewise on the magnetic field dependence of the involved valence-band level and on the position of the quasi-Fermi level.

As the energy difference between these valance-band levels varied very slowly with the magnetic field in the k_H region where they approach one

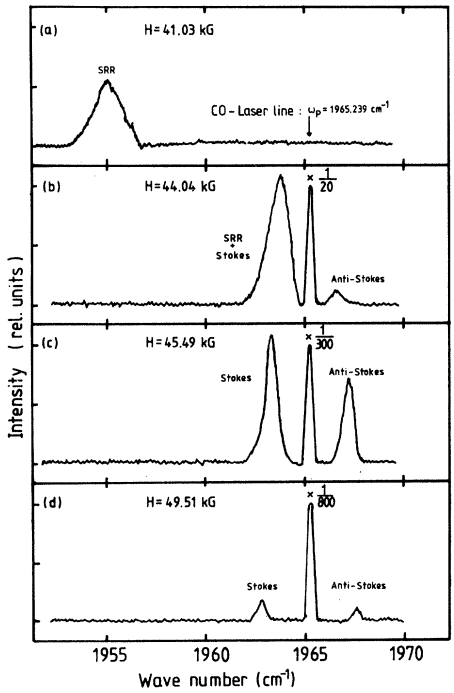

FIG. 13. Four different spectra illustrate the single phases of the stimulated Raman scattering from photoexcited holes (T=1.6 K, pump frequency ω_L=1892.263 cm^{-1}, polarization: $\vec{E}_L \| \vec{H}$).

another (see Figs. 6 and 7), the tuning characteristics of the Raman shifts are especially due to the magnetic field dependence of the quasi-Fermi level. In Fig. 13 four spectra are given which show the single phases of the scattering process. At a magnetic field of 41.03 kG the pump frequency ω_P=1965.2 cm^{-1} is completely absorbed. There is no Raman scattering possible. But the intensity of the laser radiation is high enough that stimulated recombination radiation (SRR) can be observed. The investigation of this SRR, which we interpret as band-band recombination, is given in Ref. 9. An increase of the magnetic field shifts the SRR towards the laser line. For a magnetic field of 44.04 kG [Fig. 13(b)] we observed the transmitted laser line, the stimulated anti-Stokes line, and the SRR overlapping the Stokes line. The interaction of the SRR and the stimulated radiation narrows the linewidth of the SRR. The same interaction has been observed between SRR and stimulated spin-flip Raman scattering in n-type InSb.[10] At a magnetic field of 45.49 kG there is only the stimulated Stokes, anti-Stokes, and the transmitted laser line to be seen [Fig. 13(c)]. By further increasing the magnetic field the intensities of the Stokes and anti-Stokes radiation became rapidly smaller until the scattered radiation was no longer to be seen. Both valence-band levels were then filled with electrons in the k_H region where the combined density of states has a maximum and the Pauli exclusion principle excludes the Raman transition. If you want to observe the stimulated Raman transition at higher magnetic fields you have to take a pump wavelength which has enough energy and intensity to produce the "fitting" quasi-Fermi level again. This is the reason why the tuning characteristic of the stimulated scattering process for a given excitation wavelength is only observable for 5 to 7 kG.

The population of thermal holes was very low at the temperature of 1.6 K at which the experiment had been performed. When you calculate the probability of thermally exciting an electron from the valence band to the known acceptor level (E_A = 8 meV) at 1.6 K you find a hole population of less than 10^7 cm^{-3}.

In order to estimate the photoexcited hole production by the incident laser light, we compute the photon number for the wavelengths and intensities used. For example the CO-laser line ω_P = 1947.5 cm^{-1} with a peak power of 100 W and a pulse duration of 100 nsec corresponds to the photon number of 2×10^{14}. The laser light was focused into a volume of about 3×10^{-4} cm^3 inside the InSb sample. Complete absorption of the laser light would produce about 10^{18} hole-electron pairs/cm^3.

The lifetime of the photoexcited holes is about 10^{-5} sec at low temperatures[11] and therefore remarkably longer than the duration of the laser pulse. Thus a population of about 10^{18} holes/cm^3 can be produced by the laser radiation. In the magnetic field region where the scattering process is observed, the laser radiation is almost completely absorbed so that we may expect a hole population of 10^{17} to 10^{18} holes/cm^3. This population density is high enough to produce the fitting quasi-Fermi levels of about 10 to 20 cm^{-1} which are necessary to observe the scattering process between 35 and 65 kG (see Figs. 4 and 5).

For magnetic fields smaller than 30 kG no stimulated Raman scattering from photoexcited holes has been observed, but we did observe the stimulated spin-flip Raman scattering from photoexcited electrons up to 40 kG. Figure 14 shows the magnetic field dependence of the first and second Stokes of the spin-flip Raman scattering from photoexcited electrons. The spin-flip Raman scattering from photoexcited electrons showed in almost every detail the same behavior as the well known spin-flip Raman scattering in pure n-type InSb. The gain of the photoexcited electrons spin-flip process exceeds that of the photoexcited holes scattering process and is therefore dominant in the

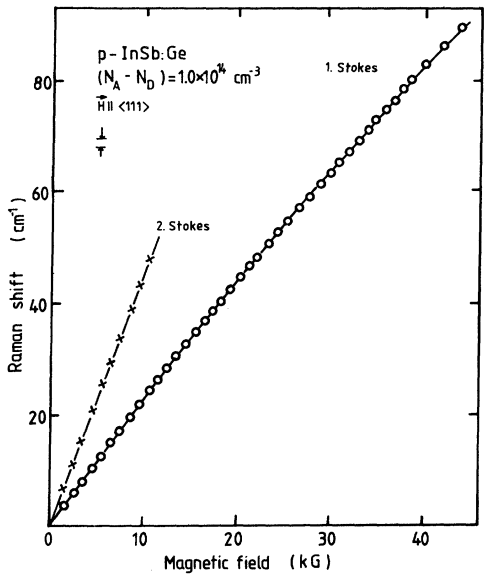

FIG. 14. Magnetic field dependence of the first and second Stokes of the spin-flip Raman scattering from photoexcited electrons.

low magnetic field region. An increase of the magnetic field leads to an increase of the combined density of states, which is linear in H [see Eq. (1)]. So, at a critical magnetic field ($\gtrsim$30 kG), the threshold for holes scattering is reached and the scattering process begins.

The temperature dependence of the hole scattering is also a question of threshold conditions. We found a dramatic increase (up to factor 5) of the Raman gain for spin-flip scattering in n-type InSb when we reduced the sample temperature from 4.2 to 1.8 K.[12] So we think that at the temperature of 2.5 K the threshold for hole scattering is no longer achieved and the transition disappears.

In all spectra only the first Stokes line and the first anti-Stokes line could be registered. For a stimulated process, the anti-Stokes line can only be generated by mixing processes. So higher Stokes lines can be expected to be generated by mixing processes, too, especially at this very small frequency shift where there is little dispersion and where the phase-matching problems can be neglected. The absence of higher Stokes lines in our spectra is to be explained as follows: The mixing process, which yields the electric field of the anti-Stokes line (E_{AS}), is given by

$$E_{AS} \sim E_L E_L E_S^* .$$

So the strong electric field of the pump laser E_L contributes twice, the electric field of the first Stokes line E_S^* contributes only once to the generation of the anti-Stokes line. In the case of the second Stokes line ($E_{2.S}$) you find

$$E_{2.S} \sim E_L^* E_S E_S .$$

Here the electric field of the pump laser contributes only once to the generation of the second Stokes line. Since in our experiment $E_L \gg E_S$, there was only the mixing process for the anti-Stokes to be observed for the given intensity of the pump laser. In a similar way you can argue the absence of higher Stokes lines.

The final aspect of the analysis of our data concerns the selection rules for the discussed hole scattering process. The polarization of the Stokes photon is the same as the polarization of the incident photon. So the observed scattering process *cannot be* a spin-flip transition according to the definition by Yafet[1] and to the selection rules given in Table II. But with the aid of the selection rules given in Table I the mechanisms for the postulated Raman transitions can be identified: For $\vec{H} \| \langle 100 \rangle$ the postulated transition $3_1 3^- 31 \rightarrow$ intermediate state $\rightarrow 1_0 1^+ 31$ is allowed in the (π, π) polarization by two-step processes of the types (M_0, M_4), (M_4, M_0), and (M_1, M_5) with the intermediate states $3_2 3^+ 11$, $1_0 1^- 11$, and $3_1 3^- 31$, respectively. (Note that the selection rules given in Table I describe electron transitions and not hole transitions.) For $\vec{H} \| \langle 111 \rangle$ the postulated transition $3_2 0^+ \rightarrow$ intermediate state $\rightarrow$ intermediate state $\rightarrow 0_0 0^+$ is allowed in the (π, π) polarization by the two-step processes of the types (M_0, M_2) and (M_1, M_3) with the intermediate states $3_2 0^-$ and $3_1 0^+$, respectively. These are the mechanisms which contribute most to the stimulated Raman scattering process we observed.

In summary, the analysis of our experimental data justifies the interpretation of the observed scattering process to be a stimulated Raman scattering process from photoexcited holes with a nonzero momentum along the direction of the magnetic field. Latest valence-band calculations allow the identification of the Landau levels involved in the scattering process. For sample orientation $\vec{H} \| \langle 100 \rangle$ the initial state is the valence-band Landau level ALH $1_0 1^+ 31$ and the final state is BHH $3_1 3^- 31$. For the orientation $\vec{H} \| \langle 111 \rangle$ initial state and final state are BLH $0_0 0^+$ and AHH $3_2 0^+$, respectively. ALH, BLH are the "light hole" ladders (approximate spin $M = +\frac{3}{2}$ and $M = -\frac{3}{2}$, respectively). AHH, BHH are the "heavy hole" ladders (approximate spin $M = -\frac{1}{2}$ and $M = +\frac{1}{2}$, respectively). In this case the initial and final states mark the position of the hole before and after the scattering process. The observation of more than eight transitions (see Fig. 10) contradicts Scott's theory but confirms our interpretation of the experimental data.

ACKNOWLEDGMENTS

We should like to thank Professor U. Rössler and Dr. H.-R. Trebin for helpful discussions about the band structure of InSb and for leaving us their calculation program to be used for the valence-band levels. The support of the Deutsche Forschungsgemeinschaft is gratefully acknowledged. Numerical calculations were performed at the Rechenzentrum der Universität Würzburg.

---

*Present address: Forschungsinstitut für Optik, Schloss Kressbach, D-7400 Tübingen, Federal Republic of Germany.

[1]Y. Yafet, Phys. Rev. 152, 858 (1966).
[2]R. L. Hollis and J. F. Scott, Phys. Rev. B 15, 942 (1977).
[3]R. Ebert, H. Pascher, G. Appold, and H. G. Häfele, Appl. Phys. 14, 155 (1977).
[4]H.-R. Trebin, U. Rossler, and R. Ranvaud, Phys. Rev. B 20, 686 (1979).
[5]J. F. Scott, Phys. Rev. Lett. 44, 1358 (1980).
[6]J. G. Hensel and K. Suzuki, Phys. Rev. B 9, 4184 (1974).
[7]C. R. Pidgeon and R. N. Brown, Phys. Rev. 146, 575 (1966).
[8]R. Ranvaud, H.-R. Trebin, U. Rossler, and F. H. Pollak, Phys. Rev. B 20, 686 (1979).
[9]H. Pascher and H. G. Häfele, Appl. Phys. 20, 75 (1979).
[10]G. Appold, W. Richter, H. Pascher, and H. G. Hafele, Opt. Commun. 15, 147 (1975).
[11]R. A. Laff and H. Y. Fan, Phys. Rev. 121, 53 (1961).
[12]H. Pascher, unpublished data.